Incorporating geologic structure into the inversion of magnetic data

Kristofer Davis
UBC-Geophysical Inversion Facility
Dept. of Ocean and Earth Sciences
University of British Columbia
6449 Stores Rd
Vancouver, BC V6T 1Z4, Canada
kdavis@eos.ubc.ca

Douglas W. Oldenburg
UBC-Geophysical Inversion Facility
Dept. of Ocean and Earth Sciences
University of British Columbia
6449 Stores Rd
Vancouver, BC V6T 1Z4, Canada
doug@eos.ubc.ca

Michael Hillier
Mira Geosciences
310 Victoria Street, Suite 309
Westmount, QC H3Z 2M9, Canada
mikeh@miragеoscience.com

SUMMARY

Magnetic field inversions are non-unique but a realistic goal is to find a causative earth structure that is compatible with the geophysical data, the petrophysical constraints, and with geology. Invariably the inversion results are improved as the number and diversity of constraints are increased. In this paper we concentrate upon the inclusion of geologic structural information. Geologic structural modelling programs can import faults, boundaries, and strike and dips of geologic units and interpolate this sparse information in space. When provided with a 3D voxel mesh, they can compute a strike, dip, and plunge for each cell. Following previous work, structural geologic information is incorporated into the inversion as a weak constraint by encapsulating it into the model objective function. The model objective function is formed such that each prism has its own set of rotated vectors to enforce smoothness along the direction of the geology. User-controlled parameters specify the degree of smoothness throughout the 3D volume and thus allow additional geologic insight to be directly incorporated. In addition to structural geology, the inversion algorithm utilizes reference models and bound constraints that help us realize our goal of incorporating all available information. The efficacy of the inversion is demonstrated through a synthetic and a field example.

Key words: magnetics, inversion, geology

INTRODUCTION

Inversion of magnetic data is difficult because of the problem of non-uniqueness. Incorporating prior information can lead the inversion algorithm to a more realistic earth structure. The ability to add knowledge of the subsurface is especially important as the depth increases and the resolution becomes limited. There has been much in the literature addressing the issue of adding geology to inversions. For example, Barbosa and Silva (1994), Bosch *et al.* (2001), Wijn and Kowalczyk (2007), and Guillen *et al.* (2008) are just a few that have directly incorporated geology in a stochastic inversion framework. Adding structural information has also been implemented in deterministic inversions (e.g. Li and Oldenburg, 2000; Lelièvre and Oldenburg, 2009) through soft constraints. It is within this foundation that we examine the practicalities of adding orientation from structural geology via the model objective function.

In this paper we begin with the description of the model objective function and how one rotates the coordinate system to enforce smoothness in a non-principle axis direction. Discretization of the structural information onto a three-dimensional voxel mesh is important and as such is discussed further. The end result is a strike, dip, and plunge (or tilt) as well as length scales for every cell. We follow the procedures given by Lelièvre and Oldenburg (2009) and discuss the assumptions and caveats for application given geologic data.

MODEL OBJECTIVE FUNCTION

Inversion is performed through a minimization of the global objective function, □, comprised of two components: the data misfit function, □$_d$, and model objective function, □$_m$:

$$\min \phi(\boldsymbol{\kappa}) = \phi_d(\boldsymbol{\kappa}) + \beta\phi_m(\boldsymbol{\kappa}) . \tag{1}$$

The data misfit function quantifies how well the forward modelled data from the inversion reproduces the observed data. The model objective function quantifies model complexity though spatial derivatives. The model objective function is defined as

$$\begin{aligned}\phi_m &= \alpha_s \int_V (\kappa - \kappa_o)^2 dv + \alpha_x \int_V \frac{\partial}{\partial x}(\kappa - \kappa_o)^2 dv \\ &+ \alpha_y \int_V \frac{\partial}{\partial y}(\kappa - \kappa_o)^2 dv + \alpha_z \int_V \frac{\partial}{\partial z}(\kappa - \kappa_o)^2 dv,\end{aligned} \tag{2}$$

where the α values place emphasis on the elongation of the recovered model for each direction and κ_o is the reference model. The reference model may or may not be incorporated into the smoothness terms (*x, y,* and *z*) but is always associated with the smallness term (*s*). It should also be noted that the required depth weighting function could be added into the model objective function or used to normalize the sensitivities. For clarity, we have chosen to do the latter. The coordinate system is right-handed with z-positive down.

To incorporate geologic structure into the model objective function a series of three sequential rotations are applied. The end result is a rotated coordinate system for equation 2 as shown in Figure 1. Equation 2 for a rotated system would be the same but where *x'*, *y'*, and *z'* are substituted for *x, y,* and *z*.

Though the coordinate system is now rotated, the actual mesh is still aligned in the principal axes. Differences across cell

faces in the *x*-, *y*-, and *z*-directions are calculated to compute the derivatives in Equation 2. A face-centred integration approach is applied to best represent *x'*, *y'*, and *z'* derivatives.

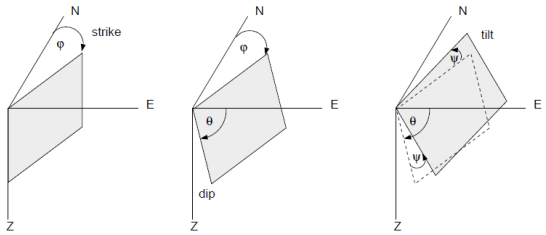

Figure 1. The rotated coordinate system as defined by, and from, Lelièvre and Oldenburg (2009) and Li and Oldenburg (2000).

For every cell, and in each mesh direction, the difference in the positive axis direction (forward) and the negative axis direction (backward) are calculated. The forward difference of is the interaction of the ith and i^{th}+1 cells. Likewise the backwards difference is the interaction of the ith and i^{th}-1 cells. The combination of these forward and backward difference operators in three dimensions and the components of the rotation matrix, create rotated matrices for the formation of the smoothness terms. The rotated matrices are given as

$$\mathbf{B}_{x,i}^{rot} = \mathbf{R}_{xx}\mathbf{D}_{x,i} + \mathbf{R}_{xy}\mathbf{D}_{y,i} + \mathbf{R}_{xz}\mathbf{D}_{z,i}; i = 1,8 \quad (3)$$

$$\mathbf{B}_{y,i}^{rot} = \mathbf{R}_{yx}\mathbf{D}_{x,i} + \mathbf{R}_{yy}\mathbf{D}_{y,i} + \mathbf{R}_{yz}\mathbf{D}_{z,i}; i = 1,8 \quad (4)$$

$$\mathbf{B}_{z,i}^{rot} = \mathbf{R}_{zx}\mathbf{D}_{x,i} + \mathbf{R}_{zy}\mathbf{D}_{y,i} + \mathbf{R}_{zz}\mathbf{D}_{z,i}; i = 1,8 \quad (4)$$

where the difference-operators matrices, **D**, are given in Table 1 and where **R** represents a diagonal matrix containing the value of the rotation matrix for that component for each cell. The rotated model objective function can be described in vector form as

$$\begin{aligned}\phi_m &= (\boldsymbol{\kappa} - \boldsymbol{\kappa}_o)^T \mathbf{W}_s^T \mathbf{W}_s (\boldsymbol{\kappa} - \boldsymbol{\kappa}_o) + \\ &\boldsymbol{\kappa}^T \frac{1}{8}\sum_{i=1}^{8}\begin{bmatrix}(\mathbf{B}_{x,i}^{rot})^T \mathbf{V}_x \mathbf{B}_{x,i}^{rot} + (\mathbf{B}_{y,i}^{rot})^T \mathbf{V}_y \mathbf{B}_{y,i}^{rot} \\ + (\mathbf{B}_{z,i}^{rot})^T \mathbf{V}_z \mathbf{B}_{z,i}^{rot}\end{bmatrix}\boldsymbol{\kappa}, \quad (6) \\ &= (\boldsymbol{\kappa} - \boldsymbol{\kappa}_o)^T \mathbf{W}_s^T \mathbf{W}_s (\boldsymbol{\kappa} - \boldsymbol{\kappa}_o) + \boldsymbol{\kappa}^T \mathbf{W}^T \mathbf{W} \boldsymbol{\kappa},\end{aligned}$$

where $\mathbf{V}_x$, $\mathbf{V}_y$, and $\mathbf{V}_z$ are diagonal matrices with cell volumes and α values for the three orthogonal directions of the mesh and the $\mathbf{B}^{rot}$ are matrices that contain the rotation matrix and discrete derivatives.

The formation of the model objective function could include the reference model in the smoothness terms (i.e. *x, y, z*) but we have chosen to only include it in the smallness term (*s*). Additionally, the eight terms are stored separately and the calculation of the model objective function consists of nine matrix-vector operations (including the smallness term), reducing computation time for the formation of $\mathbf{W}^T\mathbf{W}$ through matrix-matrix operations.

DISCRETIZATION OF GEOLOGY

The discretization of geology onto a 3D voxel mesh can be accomplished in a number of different ways. We choose to convert the planar (strike and dip) structural measurements into 3D vectors, $\boldsymbol{v}_i$. These vectors are bi-directional, i.e. vectors can be either $\pm\boldsymbol{v}$. A polarity of $+\boldsymbol{v}$ or $-\boldsymbol{v}$ is assigned to each $\boldsymbol{v}_i$. Polarity assignments are determined through the data analysis of vectors. This aspect merits further discussion and can be found in the next section. The dip field is interpolated at every cell of a 3D voxel mesh using an inverse-distance weighting scheme on the vector components associated with the structural data. It is generally accepted that two spatially close data points are more correlated than points separated by larger distances. In addition, resulting dip fields are perpendicular to the plunge calculated from the data. The dip and strike angles are calculated for every cell from the interpolated dip field. For plate-like objects, the same plunge value is set to all cells. The plunge does not have the same effect as it would for spheroid bodies that would require changing values dependent upon the geologic situation.

Sum iteration	$\mathbf{D}_x$	$\mathbf{D}_y$	$\mathbf{D}_z$
1	Backward	Backward	Backward
2	Backward	Backward	Forward
3	Backward	Forward	Backward
4	Backward	Forward	Forward
5	Forward	Backward	Backward
6	Forward	Backward	Forward
7	Forward	Forward	Backward
8	Forward	Forward	Forward

Table 1. Orientations of the finite-difference operators of each spatial direction for the eight iterations required for the model objective function.

Polarity

There are two polarity issues associated with bi-directional vectors derived from 3D structural measurements. Vector polarity is arbitrary for these vectors since they are bi-directional $\pm\boldsymbol{v}$. The first polarity issue is that dip planes in structural geology are pointing downward. If the downward polarity of the vectors is kept, fields as shown in Figure 2a are obtained. The resulting fields do not reproduce the structural trend appropriately. To produce the structural trend, comparisons of dip vectors from the collection of structural observations is completed to assign polarity to these vectors. Dip vectors on the left side are opposing the dip vectors on the right side, and vice versa. The vectors on left side of Figure 2b have their downward polarity flipped upward. As a result, a structural vector field that reproduces the expected geometry is obtained. The other polarity issue is related to the fact that these measurements are attributed with facing (Younging) directions. Facing directions give more structural information than dip directions because they provide the direction in which progressively younger stratigraphy is found in a fold. These directions are used to assign polarity to bi-directional vectors associated with the structural observations. Using the facing directions for polarity assignments can yield different field results calculated from structural observations having the same dip vectors but having different facing directions. This is illustrated in Figure 3. One of the major challenges for incorporating geologic information is assigning the polarity to vectors derived from structural measurements and using the facing direction information if that is available. Polarity

assignments of vectors are required to properly model structural fields.

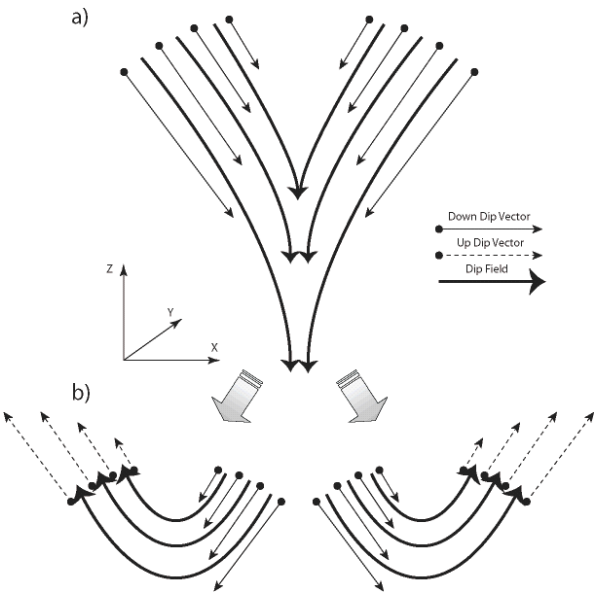

Figure 2. Polarity effect from vectors associated with structural observations on bedding fields. When the down-dip polarity (a) is kept on structural vectors, it creates an incorrect trend. Correct polarity assignments (b) to structural vectors reproduce the geometry of the expected fold structure. Both polarities in (b) are equally correct.

A reference vector is required to determine the vector polarities of dip vectors associated with the collection of structural observations. The reference vector is a normal associated with one of the structural observations. The normal associated with this particular structural observation is the normal that is closest to being perpendicular to the calculated plunge vector. It is noted that a dip plane has two normals, one for upright and one for over-turned dip planes. Once the reference vector is determined, angles on the *XY* plane between the reference vector and the normals associated with the structural observations are computed. A dip vector's polarity is flipped when the reference vector and the normal associated with the structural observation is opposing one another.

PRACTICAL APPLICATION

The α values from Equation 2 are an important component of the model objective function. Length scales are used and are easier to comprehend and incorporate than α. It is natural to use length scale values for understanding. One necessary key is the consistency of units. The derivative terms are in metres and likewise the spatial length scales are also in metres and metres squared for the smallest term. Values of α can be determined by length scales by

$$\begin{aligned} \alpha_s &= 1/\min(L_x, L_y, L_z), \\ \alpha_x &= \alpha_s L_x^2, \\ \alpha_y &= \alpha_s L_y^2, \\ \alpha_z &= \alpha_s L_z^2, \end{aligned} \tag{7}$$

and in the rotated coordinate system L_x is the length of the anomaly in the strike direction, L_y is the length in the dip direction, and L_z is the thickness of the body. Furthermore, the values of these local length scales can be incorporated for each cell. Incorporating multiple length scales allows soft constraints to decrease the derivatives edges of known features. Furthermore, data from multiple bodies are often inverted and the anomalies vary in dimension. Utilizing local length scales can thus add further soft constraints that ultimately create a more geologically acceptable inversion result. The resulting model objective function calculated in Equation 6 therefore requires six values per cell: the strike, dip, plunge (or tilt), and three length scales. Next, we introduce an example with an anticlinal sheet and a prism. A cross section of the model is shown in Figure 5a.

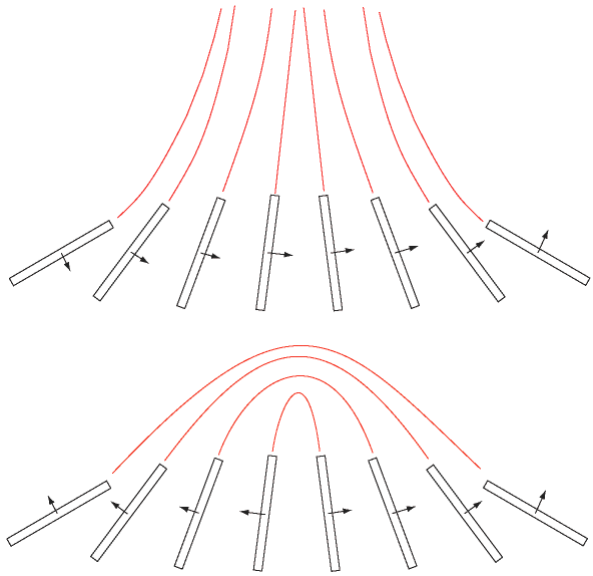

Figure 3. Facing direction utilized in structural field calculations. Two neighbourhoods of structural observations have the same dip vectors but different facing directions. (Top) All facing directions are "facing" the same direction - to the right. (Bottom) Some facing directions are opposing each other.

The data containing 2 nT of random noise are plotted in Figure 4. A typical inversion yields the low-amplitude, smooth results (Figure 5b). We now introduce the geologic structure for the volume obtained from the structural modelling package. A cross-section of the dip is presented in Figure 5c. It should be noted that the dip changes direction at the top of the fold and the strike changes from out of the page to into the page. Strike and dip information are incorporated into the model objective function. Further, length scales are adjusted so that they are small (less than a cell width) outside the general region of the anticline). The values within the region of the anticline are kept constant with the true strike and dip of the body (140 m and 45 m, respectively). The inversion is carried out (Figure 5d) and the anticlinal geology is well imaged. The quality of result is crucially dependent upon the assignment of the length scales. For instance, an inversion carried out by applying the large length cells only to the cells defining the true anticline yields the image in Figure 5e. Proper length scales are given within the anticline, and they vary with the distance of the cell to the edge of the body for each direction. Length scales of one cell width are given for the edges of the body and six cell widths for the middle of the body. Not only is the shape of the anticline recovered but so

too is the amplitude of the susceptibility. The recovered values for the anticline are close to the true susceptibilities and the recovered block is of low amplitude as expected. No additional length scales were adjusted for the prism to the west. It should also be noted that positivity was enforced and a zero reference model was provided as prior information for each inversion.

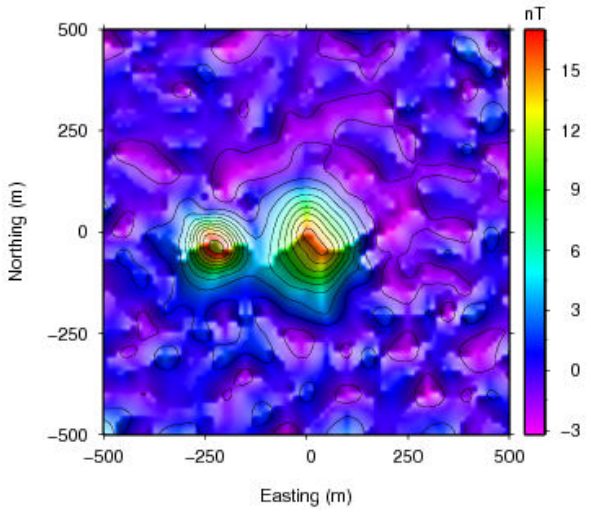

Figure 4. The observed data created from a block to the west and an anticlinal sheet in the centre. A cross-section of the model is given in Figure 5a.

CONCLUSIONS

Structural information can supply an inversion of magnetic data with soft constraints to drive the recovered model towards the known geology. Each cell is provided with 6 additional parameters: the strike, dip, and plunge to specify orientation and three length scales which provide a scale for the structure with which the cell is affiliated. This information can be extracted from a structural geologic model.The use of normals keep the geology consistent with the assumptions made in the geophysics. The use of bound constraints and reference models can further add information for the recovery of a model that agrees with both the geology and geophysics.

ACKNOWLEDGMENTS

We thank Peter Lelièvre and Nick Williams for helpful discussions on the model objective function.

REFERENCES

Bosch, M., A. Guillen, and P. Ledru, 2001, Lithologic tomography – an application to geophysical data from the Cadomian belt of Northern Brittany, France: Tectonophysics, 331, 197–227.

Barbosa, V. C. F., and J. B. C. Silva, 1994, Generalized compact gravity inversion: Geophysics, 59, 57–68.

Guillen, A., Ph. Calcagno, G. Courrioux, A. Joly, and P. Ledru, 2008, Geological modelling from field data and geological knowledge, Part II, Modelling validation using gravity and magnetic data inversion: Physics of the Earth and Planetary Interiors, 171, 158–169.

Lelièvre. P. G. and D. W. Oldenburg, 2009, A comprehensive study of including structural orientation information in geophysical inversions: Geophysical Journal International, 178, 623-627.

Li, Y. and D. W. Oldenburg, 2000, Incorporating geologic dip information into geophysical inversions: Geophysics, 65, 148–157.

Wijns, C. and P. Kowalczyk, 2007, Interactive geophysical inversion using qualitative geological constraints: Exploration Geophysics, 38, 208–212.

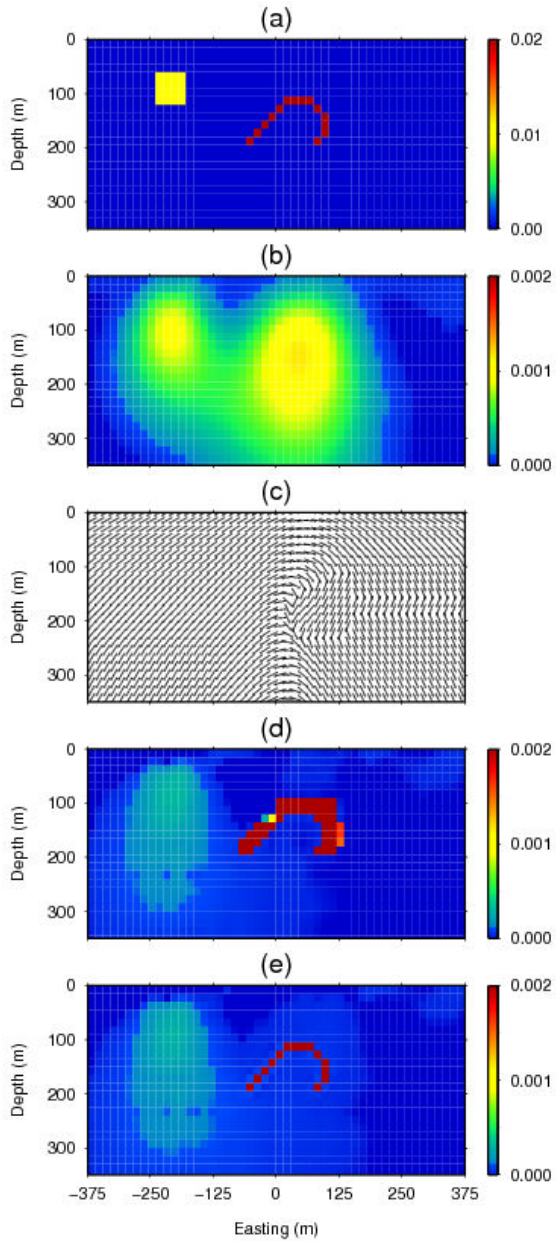

Figure 5. A cross-section of the true model is shown in (a). A typical inversion result with no dip information is shown in (b). The dip information (c) is given via the model objective function and its respective length scales. The recovered model in (d) represents close guess to the true geology. The recovered model incorporating true, known local length scales is in (e). The colour scales are the same in (b), (d) and (e) for comparison. All plots are cross-sections of a 3D model.